Journal of Electrochemistry

Volume 25
Issue 2 *Special Issue: Electrochemical Analysis and Sensing (I)*

2019-04-28

In Situ/Operando Visualization of Electrode Processes in Lithium-Sulfur Batteries: A Review

Shuang-yan LANG

Xin-cheng HU

Rui WEN
Key Laboratory of Molecular Nanostructure and Nanotechnology, Beijing National Laboratory for Molecular Sciences, CAS Research/Education Center for Excellence in Molecular Sciences, Institute of Chemistry, Chinese Academy of Sciences (CAS), Beijing 100190, China;University of Chinese Academy of Sciences, Beijing 100049, China;, ruiwen@iccas.ac.cn

Li-jun WAN
Key Laboratory of Molecular Nanostructure and Nanotechnology, Beijing National Laboratory for Molecular Sciences, CAS Research/Education Center for Excellence in Molecular Sciences, Institute of Chemistry, Chinese Academy of Sciences (CAS), Beijing 100190, China;University of Chinese Academy of Sciences, Beijing 100049, China;, wanlijun@iccas.ac.cn

Recommended Citation

Shuang-yan LANG, Xin-cheng HU, Rui WEN, Li-jun WAN. *In Situ/Operando* Visualization of Electrode Processes in Lithium-Sulfur Batteries: A Review[J]. *Journal of Electrochemistry*, 2019 , 25(2): 141-159.
DOI: 10.13208/j.electrochem.181048
Available at: https://jelectrochem.xmu.edu.cn/journal/vol25/iss2/2

DOI: 10.13208/j.electrochem.181048 **Artical ID**:1006-3471(2019)02-0141-19
Cite this: *J. Electrochem.* **2019**, *25*(2): 141-159 **Http**://electrochem.xmu.edu.cn

In Situ/Operando Visualization of Electrode Processes in Lithium-Sulfur Batteries: A Review

LANG Shuang-yan[1,2], HU Xin-cheng[1,2], WEN Rui[1,2*], WAN Li-jun[1,2*]
(1. *Key Laboratory of Molecular Nanostructure and Nanotechnology, Beijing National Laboratory for Molecular Sciences, CAS Research/Education Center for Excellence in Molecular Sciences, Institute of Chemistry, Chinese Academy of Sciences* (*CAS*), *Beijing* 100190, *China*; 2. *University of Chinese Academy of Sciences, Beijing* 100049, *China*)

Abstract: Lithium-sulfur (Li-S) batteries have been regarded as one of the most promising candidates for the next-generation energy storage devices. Fundamental understanding of the structure and evolution processes at electrode-electrolyte interfaces is essential to the further development. In this review, we summarize recent advances in the interfacial observations by means of various *in situ/operando* visualization techniques, including scanning probe microscopy (SPM), electron microscopy (EM), X-ray microscopy (XRM) and optical microscopy (OM). The real-time investigation provides important evidence for the morphology and component changes including S/Li_2S transformation, polysulfide dissolution on cathodes and Li/solid electrolyte interphase (SEI) evolution on anodes, which presents reaction mechanism and design principles for Li-S battery optimization.

Key words: *in situ* visualization; Li-S batteries; electrode-electrolyte interface; Li anode; electrode processes
CLC Number: O646 **Document Code**: A

Energy availability in a reliable and environmentally responsible way holds the key to achieving a sustainable world. The ever-growing demands imposed by modern consumer electronics, automotive industries and electrical grid require great advances in the renewable energy generation and storage technologies. As the low specific energy of current commercial lithium-ion batteries (LIBs) is insufficient for the long-term needs, "beyond lithium-ion" energy storage systems with high energy densities are enthusiastically pursued. Among these, lithium-sulfur (Li-S) batteries have drawn widespread attention because of their high theoretical energy density of 2600 $Wh \cdot kg^{-1}$. And, elemental sulfur is naturally abundant, inexpensive and nontoxic, making Li-S batteries very relevant to the safe and green life[1-3].

Nevertheless, there are still some challenges hindering the practical applications of Li-S batteries. During Li-S electrochemical reactions, S is reduced through a sequence of sulfide products, $n/8S_8 + 2e \Leftrightarrow S_n^{2-}$, $S_n^{2-} + (2n-2)e \Leftrightarrow nS^{2-}$ ($4 \leqslant n \leqslant 8$) corresponding to the conversion from S to intermediate polysulfides (PS) and Li_2S[4]. The S and discharge products of Li_2S_2 and Li_2S are insoluble and electrically insulating, which impedes the electrochemical accessibility upon discharge/charge. The intermediate PS dissolve and diffuse in the electrolyte, inevitably resulting in the loss of active materials and the corrosion of Li anode. Moreover, the short-chain PS can move back to the cathode and be re-oxidized to long-chain PS. These parasitic reactions occur continuously known as the "shuttle effect", which renders the self-discharge process and low Coulombic efficiency[5-6].

On the Li anode, the formation of the solid electrolyte interphase (SEI) is a "double-edged sword". On one hand, it protects the Li anode from the physi-

Received: 2018-12-14, Revised: 2019-01-08 *Corresponding author, Tel: (86-10)82613081, E-mail: ruiwen@iccas.ac.cn, wanlijun@iccas.ac.cn

cal contact with the electrolyte, avoiding the superfluous reduction of electrolyte components. On the other hand, the formation of SEI layer intrinsically consumes the electrolyte. Actually, the composition of SEI is always nonuniform, which leads to the nonuniform ionic conductivity and therefore localized electrodeposition of Li metal. This nucleation of Li dendrite will give rise to the instability and safety issues. Besides, upon the stripping/plating of the protuberances, the interfacial impedance is increased due to the repeated formation of dead Li and new SEI[7-8]. Understanding the properties and behaviors of the electrode-electrolyte interfaces during electrochemical processes is the necessary prerequisite to the efficient interfacial engineering on both electrodes.

Significant progress has been made in the in-depth understanding of the interfacial mechanism in Li-S batteries. Traditional *ex situ* techniques have provided useful information in terms of morphology and chemical components in spite of their drawbacks in post treatments and the time decay. Constructively, *in situ* characterization techniques are employed [9]. They can capture the real-time information inside working batteries, which omits the post-treatment processes with external disturbances. In Li-S batteries, *in situ* spectroscopic characterization techniques, such as Raman spectroscopy, ultraviolet visible (UV-Vis) absorption spectroscopy, X-ray absorption near-edge structure (XANES), nuclear magnetic resonance (NMR) and high-performance liquid chromatography (HPLC), mainly focus on the detection of the evolution for the dissolved PS. Meanwhile, the microscopic characterization techniques pay more attention on the morphology and structure changes of the solid products on electrodes, which directly visualize the electrode-electrolyte interfaces for the in-depth mechanism understanding[10-11]. Important reviews have summarized the *in situ*/*operando* characterization techniques, mainly of spectroscopic methods, for rechargeable Li-S batteries [12-13]. In complementary fashion, our review is written with an eye to *in situ*/*operando* visualization of the electrode processes in Li-S batteries.

In this review, *in situ*/*operando* visualization techniques for Li-S batteries are summarized according to the unique applications and imaging principles, including scanning probe microscopy (SPM), electron microscopy (EM), such as transmission electron microscope (TEM) and scanning electron microscope (SEM), X-ray microscopy (XRM) and optical microscopy (OM) (Fig. 1). Using *in situ* atomic force microscopy (AFM), surface analysis of the sulfide and SEI evolution can be acquired at nanoscale under various environmental conditions, which reveals the electrolyte-dependent interfacial mechanism and a straightforward structure-reactivity correlation. The *in situ* EM techniques have been regarded as one of the most powerful tools extensively used for battery research. They highlight the observation of the morphology evolution and structure changes, playing crucial roles in the discoveries about the encapsulation and phase separation of S/Li_2S, and Li plating behaviors in Li-S batteries. The XRM techniques map the element distribution, and lay emphasis on the identification of S species and their dissolution/reformation during electrochemical cycling. In addition, although the low spatial resolution, OM is the simplest and most convenient technique suitable for modeling the entire interface rather than a few molecules or clusters, showing satisfactory effects on the observations and optimizations of Li deposition processes. While there are great advances, there are still fuzzy regions in Li-S batteries remained to be explored. Researchers should rationally utilize the advantages of the techniques, providing fundamental understanding of the reaction mechanism, as well as valuable guidance and assist for the development of new electrode materials and electrolytes. Therefore, a visual Li-S world is opened up and becoming clearer.

1 Scanning Probe Microscopy

By measuring the tip-sample interaction, AFM could provide three-dimensional (3D) information with nanoscale spatial resolution of the topography, as well as mechanical, electrical and adhesive properties under various experimental modes. Besides, *in situ* investigation can be achieved by electrochemical

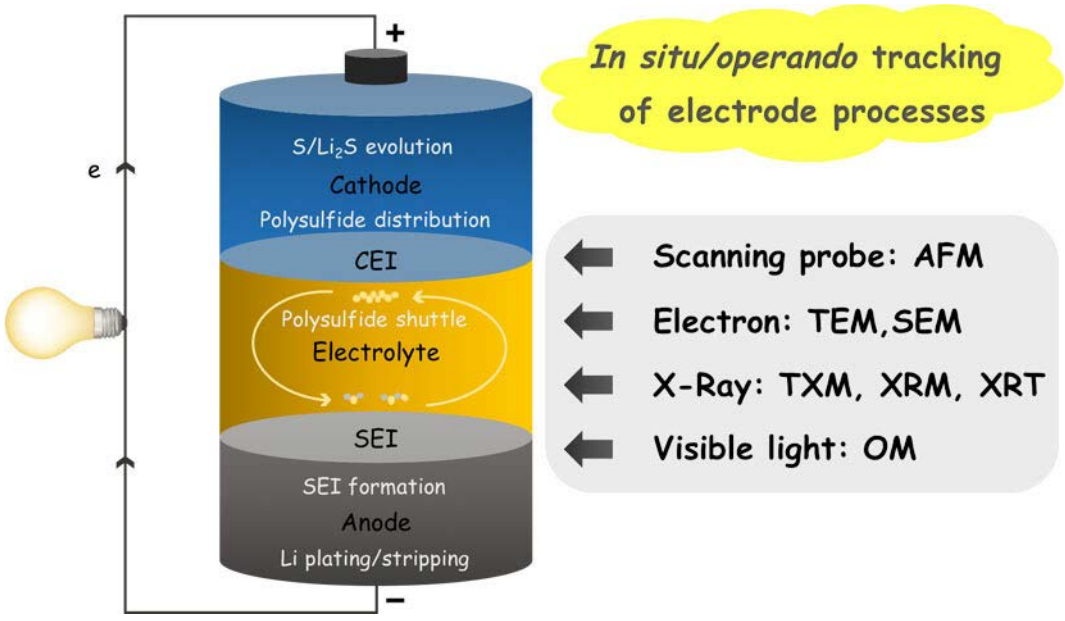

Fig. 1 Schematic representation of the *in situ*/*operando* visualization techniques for the electrode processes in Li-S batteries.

AFM (EC-AFM). The high-resolution imaging coupled with the multifunctional detection of AFM makes it useful for monitoring the electrode-electrolyte interfaces in battery systems. As the schematically shown in Fig. 2A I, the three-electrode cell is constructed, which can be then assembled on the commercial AFM for *in situ* EC-AFM observation[14]. With the experimental conditions mimicking the real electrolyte environments in Ar-filled glove box, *in situ* AFM can give direct insight into the interfacial mechanism and guidance for optimizing of Li-S batteries.

For Li-S electrochemical reactions, lithium strips were employed as the counter and reference electrodes, and HOPG was selected as the working electrode using Li_2S_8 as the catholyte. Then, interfacial evolution of the solid discharge products can be observed upon cycling. As shown in Fig. 2A II-V, nanoparticle (NP) nuclei begin to grow at 2 V during discharge, followed by the lamella sediment deposition at 1.83 V in the typical ester-based electrolyte of lithium bis (trifluoromethanesulfonyl)imide (LiTFSI) in 1,3-dioxolane/1,2-dimethosyethane (DOL/DME). Combined with the *ex situ* spectroscopic characterizations, the NPs and lamella deposits can be identified as Li_2S_2 and Li_2S, respectively. The galvanostatic precipitation of Li_2S_2 and/or Li_2S was further performed with different current rates, revealing the relationship between the interfacial reaction and battery performance. Besides, the high-temperature effect on the Li-S electrochemistry was investigated in lithium bis- (fluorosulfonyl)imide (LiFSI) electrolyte[15]. Upon discharge at 60 ℃, an *in situ* formed film can be detected (Fig. 2B), attributed to a LiF net capturing PS intermediates. This high-temperature and *in situ* formation of the functional film is of benefit to constrain sulfides from dissolving and diminish the Li^+ transport distance between the long- and short-chain PS, protecting the Li-S rechargablity and electrode conductivity after cycles. Furthermore, the Li salt mediated reaction mechanism of Li_2S deposition was discovered in LiTFSI-LiFSI binary salt electrolyte [16]. During discharge, the LiFSI causes the 3D spherical Li_2S growth, and LiTFSI induces 2D lamellar Li_2S. Interestingly, during charge, the distinct pathways of Li_2S decomposition were clearly tracked on the two distinguishing structures, shown as edge-to-center mode of lamellar Li_2S and center-to-edge of spherical (Fig. 2C). Based on the experiments above, interfacial process and reaction mechanism, as well as the effects of high temperature and Li salts in Li-S electrochemistry are presented at nanoscale using *in situ* AFM, contributing to the novel design of Li-S batter-

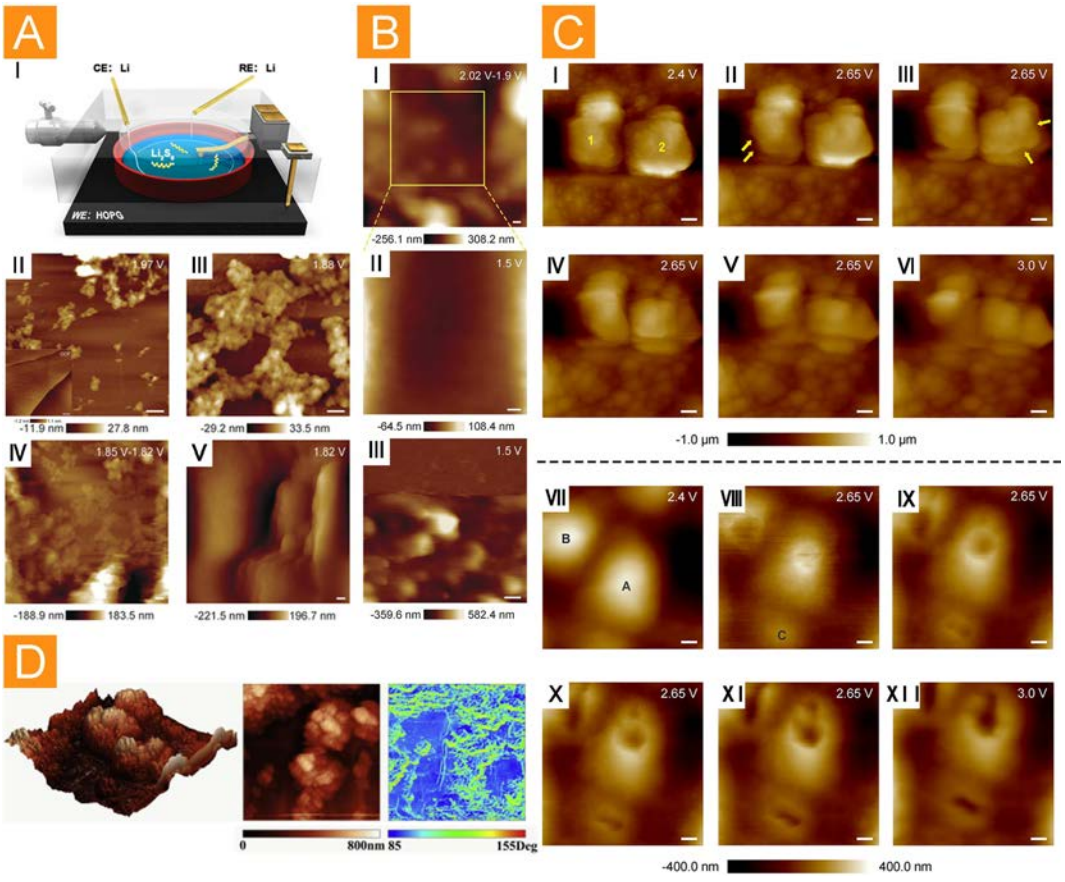

Fig. 2 (A I) Schematic of the three-electrode EC-AFM cell, *in situ* AFM images of (A II-V) the sulfide evolution at room temperature (Scale bar: 100 nm)[14], (B) the functional film formation at 60 °C upon discharge (Scale bar: 250 nm in I-II and 1 μm in III)[15], (C) lamellar and spherical Li_2S decomposition upon charge (Scale bar: 1.5 μm in I-VI and 500 nm in VII-XII)[16], (D) Li metal immersed in Li_2S_6/DOL/DME[17].

ies.

On Li metal anode, AFM was performed to compare the surface morphologies of Li samples immersed in different electrolytes[17]. As shown in Fig. 2D, the sample immersed in the electrolyte containing Li_2S_6 has randomly-distributed particles forming a rough surface. However, a smooth and homogeneous film can be obtained in $LiNO_3$/DOL/DME. This difference is ascribed to the different reactions between Li metal and the electrolytes. It is suggested that the formation of a compact and homogeneous surface film on Li anode is significant to construct the stable SEI layers for Li-S batteries.

2 Electron Microscopy on Cathode Materials

In an attempt to adapt the insulating nature of S, the primary approach has been to confine S into nanostructured conductive hosts. Theoretically, the volume expansion of S during lithiation is ≈80% which is so high that may destroy the delicately designed structure of S cathodes. Understanding the Li-S processes inside the complex cathodes is essential to estimating the performance, which can be realized by *in situ* TEM. In 2014, the lithiation of a small S particle was visualized by *in situ* TEM[18]. The Li anode reacts with S at the interface immediately after the connection. A new Li_2S crust is formed on the bulk S, revealing that the Li-S reaction is through surface diffusion. The insulating Li_2S layer makes the radial diffusion of Li^+ into the S bulk difficult. This, in turn, verifies the importance of employing the conductors to make full use of the S.

Nitrogen doped mesoporous-hollow carbon nanospheres (NMHC) were synthesized to infiltrate S[19].

And the lithiation process of NMHC-S was recorded using *in situ* TEM (Fig. 3A). With the extension of lithiation time, the volume of the particles increases gradually, indicating that the S will slightly overflow from the carbon shell. Closely packed small particles form after the lithiation, which are Li_2S crystals demonstrated by the diffraction signals. Note that the pore size of the NMHC affects their S confining ability. By comparison among the 4.1, 3.2 and 2.8 nm, the small pore size of 2.8 nm is more helpful to protect S from the electronic beam and mitigate the sublimation of S under TEM. Afterwards, loading S with porous carbon nanofibers (PCNFs) was further investigated[20]. Similar to the conclusion from the previous work, the PCNF/S electrode with micropores is the optimized choice compared to that with mid-sized mesopores, which owns a relatively large pore volume and surface area. The *in situ* TEM shows that the former electrode confines Li_2S with a low volume expansion of ≈35% upon lithiation. The structural stability of the cathode is maintained with no fracture of the carbon host. In contrast, the electrode with mesopores presents damaged/open carbon spheres, inducing the sublimation of S, a larger volume expansion of over 61%, and overflowing of Li_2S. The evolution of local structures correlates to the electrochemical performance, which offers potential strategies for stable cathodes.

In 2015, the lithiation insertion into S within cylindrical inner pores of individual carbon nanotubes (CNTs) was first monitored by *in situ* TEM[21]. As shown in Fig. 3B, the reaction front is flat, suggesting the sufficient electrical conductivity at the Li_2S/S interfaces. Additively, the mechanical strength of the produced CNTs is evidently high since no obvious expansion can be observed. The extra volume needed is accommodated by squeezing out both fillers toward the ends of the CNT vessel. Besides, the lithiation of an Fe-S@CNT material was traced using *in situ* TEM[22]. The size of the Fe-S NPs increases due to the lithiation of Fe-S to nano-Fe and Li_2S. The results reveal that CNTs not only play a crucial role in accommodating the volume expansion, but also provide fast Li^+ transport paths. Recently, *in situ* TEM was utilized to understand the lithiation dynamics in a single S-graphene nanocage (S-GNC) particle hosting both cyclo-S_8 and smaller S molecules (S_2-4)[23]. S_8 is partially filled in the inner cavity, and S_2-4 circumventing dissolved PS in the shell. The graphene shells expand homogeneously with the full lithiation of all the S molecules. More importantly, the shell expands toward inside instead of outside, implying its excellent mechanical strength. Apart from the S-C materials, *in situ* TEM had been done on MoS_2-encapsulated S spheres[24]. Owing to the internal void spaces between MoS_2 wrinkles/S cores and the hollow space within S spheres, the morphology change is highly reversible during the lithiation and delithiation processes, leading to the benign electrode-electrolyte interface and the improved long-term cycling performance. And, detailed analysis of the lithiation behavior was performed, estimating that the total Li diffusivity in the encapsulated S was around $10^{-17} \sim 10^{-16}$ $m^2 \cdot s^{-1}$. *In situ* TEM also contributes to the research on the observation of Li_2S delithiation[25]. For the Li_2S@graphene nanocapsules, after the first delithiation, the volume shrinking ratio is around 20%, which maintains small during the following cycles. This excellent structural stability guarantees the good cycle performance of the Li_2S@graphene even at high rates.

From the above results, *in situ* TEM has exerted its advantages in understanding the morphology change and reaction pathway of the various conductive materials encapsulating S upon discharge/charge, explaining the capacity fading mechanism and providing supporting information in the optimizing strategies. However, it should be mentioned that, all of the above experiments seal solid-state Li-S batteries in the *in situ* TEM chambers, which is different from the liquid environment in practical batteries. The real-time observation with the presence of the electrolyte has been an enormous challenge for studying Li-S battery reactions with the TEM. Last year, Cairns et al. employed the graphene liquid cell (GLC) -TEM technique to understand the lithiation behavior

of a cetyltrimethylammonium bromide-modified S-graphene oxide-carbon nanotube (S-GO-CTA-CNT) nanocomposite in the electrolyte of LiTFSI in DOL/DME[26]. As the *in situ* TEM images shown in Fig. 3C, Li_2S nanocrystals gradually grow and merge with newly appearing ones during lithiation. In addition, the size and position of the hole (blue arrow) on S-GO-CTA-CNT flake does not significantly change, which may indicate the homogeneous formation of Li_2S and the structural-integrity maintenance of the composite nanoarchitecture. This research on the nucleation and growth of the Li_2S nanocrystals corresponds to the results by *in situ* AFM, opening a new window for the Li-S investigation under TEM.

One more point, no bulk intermediate phases of PS can be observed in these *in situ* TEM works. It is still uncertain whether PS form prior to Li_2S, or S reduces directly to Li_2S. To clarify this lithiation mechanism, Zhang et al. obtained electron energy loss spectra (EELS) on the lithiation product of Li_xS (Fig. 3D)[27]. The low-loss EELS confirm the lithiation occurrence. Based on the core-loss EELS, the Li_xS product is ascribed to a composite of Li_2S and S, since the EELS of the PS are vastly different from the results of Li_xS, suggesting the direct transformation of S to Li_2S without intermediate PS. Given that the vacuum environment and the electron beam may impact the reaction pathways and change the phase transformation kinetics, these *in situ* TEM findings should not be generalized while still providing insightful understanding of the novel design and electrochemical mechanism in Li-S batteries.

Another work developed an electrochemical microcell for *in situ* SEM study over the delithiation of Li_2S cathodes (Fig. 3E)[28]. The Li_2S particles become smaller and smaller upon charging due to the PS dissolution into the electrolyte. This phenomenon supports that Li_2S is converted to PS chemically upon charging, which is further affirmed by the *in situ* TEM study in the ionic liquid electrolyte. Lately, many research groups have targeted solid-state batteries to minimize Li dendrite growth and safety hazards[29]. *In operando* SEM vis ualized the morphology changes, charge/discharge mechanism and the aging behavior of the all-solid-state Li-S battery employing a solid-state polymer electrolyte[30]. In Fig. 3F, needle-like products grow at the electrode-electrolyte interface after discharge. As a consequence, pores increase in the solid electrolyte, hindering the ionic/electronic conduction. Upon charging, the increase of the polymer-electrolyte brightness can be attributed to the increasing concentration of S in the electrolyte. It is shown that, at the end of charge, the image is still brighter than that in the discharge state, indicating that the PS remain and do not participate in the charge reaction. The development of *in situ* EM techniques has successfully assisted us to understand the phase transformation, volume expansion/contraction and the dynamic evolution of the cathode materials in Li-S batteries. Valuable insights into the reaction mechanism can be continuously brought accompanied by the rise of the next-generation Li-S batteries.

3 Electron Microscopy on Anode Materials

Li metal has been a promising candidate as the anode material due to the high theoretical capacity (3860 $mAh \cdot g^{-1}$) and the lowest reduction potential (-3.040 V vs. the standard hydrogen electrode). Although considered as the "holy grail", Li anode is prone to dendrite growth upon repeated stripping/plating, causing capacity loss and short circuiting. Obtaining the detailed understanding of the interfacial processes including the initial nucleation of Li dendrite, the evolution and dynamics of Li growth/dissolution, the SEI formation and the complex factors from the external environment, is the key step to address the concerns and achieve practical use of Li metal batteries.

Using *in situ* TEM, Li deposition and dissolution at the interfaces between a Pt working electrode and $LiPF_6$/propylene carbonate (PC) electrolyte can be visualized and quantificationally analyzed[31]. Images of the interface during the first charge/discharge cycle are shown in Fig. 4A. The initial deposition takes place on the smooth Pt electrode which is in favor of the uniform Li distribution on the surface.

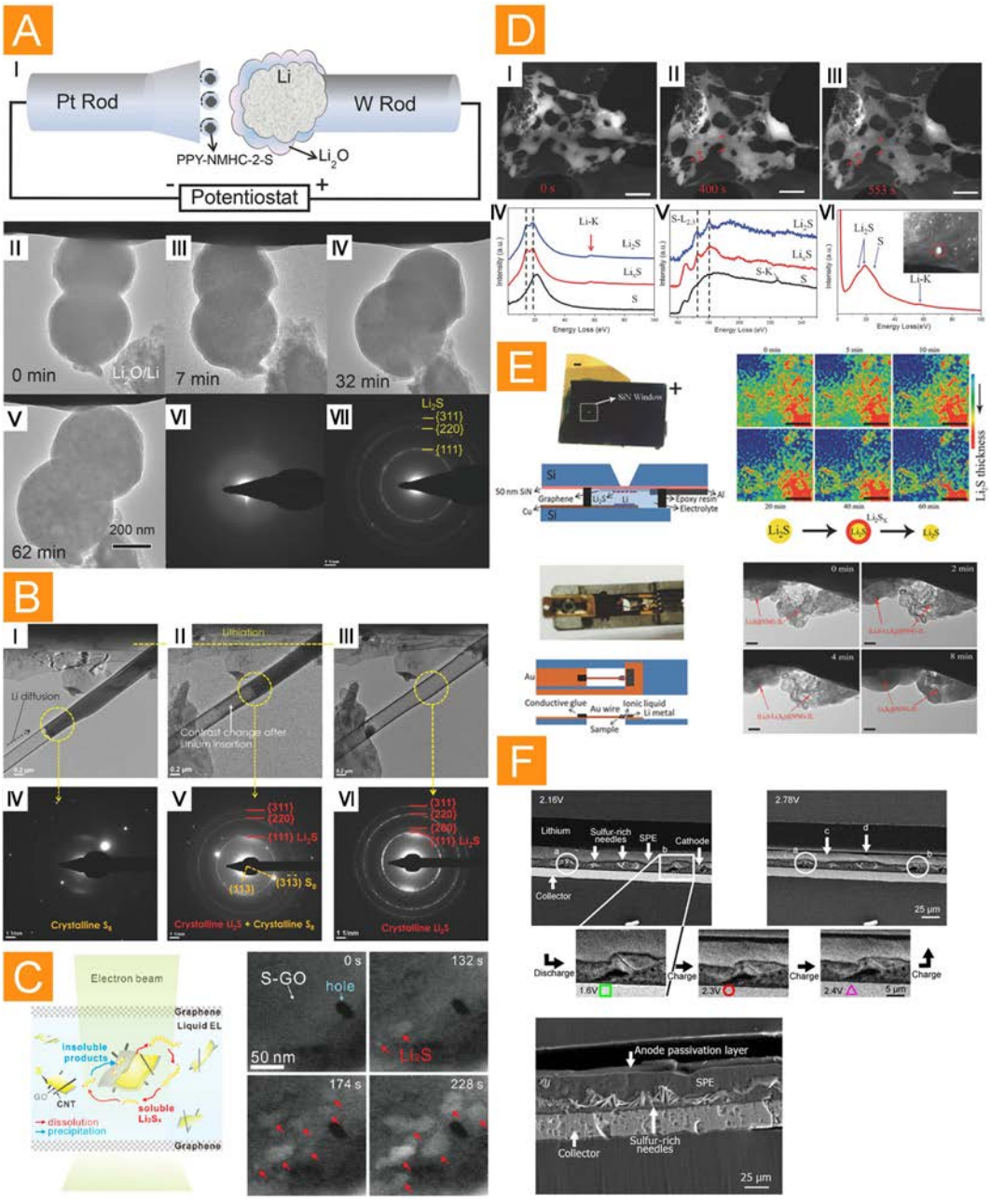

Fig. 3 (A) Schematic of the *in situ* TEM testing, *in situ* TEM images of polypyrrole coated NMHC-S during lithiation process and the diffraction mode[19]. (B) TEM images during lithiation of S nanoconfined in a CNT reaction vessel and their corresponding electron diffraction patterns[21]. (C) Schematic of *in situ* GLC-TEM technique and time-series STEM images[26]. (D) Annular dark field (ADF)-STEM images and EELS spectra of S and lithiated S samples[27]. (E) *In situ* EM set-ups and the characterization results during delithiation of Li_2S. Scale bars are 20 μm for the SEM images and 50 nm for the TEM images[28]. (F) SEM images of the Li-S cell in the discharged and charged states[30].

However, the dissolution of Li is not perfectly reversible, increasing the surface roughness, and therefore, resulting in the uneven deposition during the subsequent cycles. The contrast of Li and the electrolyte allows the direct quantification of Li from the images. As a first approximation, the amount of Li is linearly associated with the net charge density, which can be used as the figure of merit for the stability of the electrode-electrolyte interface. Besides, Leenheer et al. investigated the galvanostatic Li electrodeposi-

tion on Ti electrode in the electrolyte of $LiPF_6$ in ethylene carbonate (EC)/dimethyl carbonate (DMC)[32]. Cycling at current densities from 1 to 25 mA·cm^{-2} leads to the variations in grain structure. It is shown that the Li dendrite with the needle-like structure forms more readily at the higher current density and during the later cycles. Additionally, the effect of the electron beam was explored. The Li deposition morphology and kinetics can be changed because of the exposure to the electron beam. And a beam-induced surface film forms on Li, altering the local flux of Li^+ and the Li microstructure.

Recently, using *in situ* TEM, the root/surface growth behaviors of Li were presented in LiTFSI in dimethyl sulfoxide (DMSO)[33]. In practice, the relationship between the SEI formation and the Li deposition rates determines the surface or root growth mode, which is related to the electron competition from Li^+ and the electrolyte solvents. The surface growth mode always occurs at low overpotentials. Spherical Li grows in width as well as length, ending up with the cauliflower morphology. This is attributed to the preferred Li^+-electron interaction. The SEI exists as patches here and there, which cannot seal up the growth front. Li will grow around them, therefore forming a mixture. However, if the competition favors the latter, the SEI layer may connect and cover up the entire surface. The Li^+ diffusion is limited by the short-range solid-state transport through the SEI layer. And, the continuous growth and thickening of SEI increases its mechanical strength, constraining the Li growth physically with the stress build up from the root. When the stress reaches a threshold, root growth bursts as can be seen in Fig. 4B. Thereafter, the stress buildup/release repeats, causing the intermittent root growth with the kink formation. The SEI is thinner on the root region because of the time lag between the formation on the tip and root segments. Then the dissolution takes place primarily on the root region, leaving the tip isolated during stripping. Note that apart from the applied potential, various factors, such as the electrolyte additives and electrode materials, can affect the relative rates of Li deposition and SEI formation. In-depth understanding of their effects on Li deposition mechanism and rate is highly needed for the development of Li metal batteries.

The interfacial observation of Li behaviors by *in situ* SEM could trace back to 1990s. In a semi *in situ* mode, the influence of the current density on the morphology of Li was studied in 1998 in the plastic Li batteries[34]. From the cross-section images, it is concluded that the low current density leads to a mossy Li deposition. At higher current densities, the deposits become dendrites, which is consistent with the *in situ* TEM results. With the similar SEM measurement, Aurbach et al. investigated the Li surfaces in different electrolytes earlier[35-36]. Afterwards, Dolle et al. reported *in situ* SEM observations of Li dendrite formation in polymer batteries[37]. The cross-section images indicate the role of the dendrites on delamination between the substrate and the polymer, with the overall result being a contact loss. In 2013, the morphology changes at the Li phosphorus oxynitride glass electrolyte (LiPON)/Cu current collector interface were visualized by *in situ* SEM[38]. Needle-shape dendrite forms during Li plating. The Li on the core and root regions deflates and dissolves preferentially, resulting in the inactivity of the residual precipitates. This phenomenon verifies the above-mentioned root growth mode from *in situ* TEM, providing more information in the remained SEI husk after stripping and the interfacial morphology at large scale.

As the Li growth is greatly affected by the additives in the electrolyte, systematical study was conducted on the interfacial evolution in ether-based electrolytes with $LiNO_3$ and/or PS by *in situ* electrochemical SEM (EC-SEM)[39]. The dendrite can be suppressed in the LiTFSI/DOL/DME electrolyte with the addition of both Li_2S_8 and $LiNO_3$ (Fig. 4C). The calculation results show that Li atoms will be more energetically favorable to stay in PS clusters than in Li metal. Therefore, the deposition rate of Li is decelerated, revealed as the etching effect of PS on Li dendrites. Besides, Wang et al. recently realized the controlled deposition of Li metal via designing electrodes

with appropriate micro-/nano-architecture. By SEM investigation, they found that Li metal preferred to be deposited into the grooves of micro-/nano-patterned Ti foil, Si wafer and ZnO electrodes. The enhanced electric field near the pits guides the Li deposition, which opens up new avenues to promote the commercialization of Li metal batteries[40]. Using *in situ* EM, the clear observations of Li dendrite growth and suppression are achieved in various liquid environments and experimental conditions, providing fundamental understanding and electrolyte-optimization strategies for Li dendrite growth.

Although the characterizations have shed light on the Li behaviors, the researchers need to further solve for the Li dendrite issues and improve the Li anode cycling performance. Effective approaches have been reported, such as the rational design of nanomaterials for regulating Li upon lithiation, interfacial engineering by *in situ*/*ex situ* protection and useful reformation over the current collectors and separators[41-42]. With the aid of *in situ* TEM, the successful control of Li growth can be directly observed. For example, an interfacial layer of interconnected hollow carbon nanospheres was described to help isolate Li deposition and reduce dendrite growth by Cui et al[43]. The *in situ* TEM images recorded the morphology evolution. The deposited Li lifts up the carbon nanospheres during Li plating, which visually confirms the concept of depositing Li underneath carbon while maintaining a stable SEI with integrity. Furthermore, they deposited Li on various metal substrates[44]. A substrate-dependent growth mode is unraveled based on the different solubility of the metal materials in Li. During Li deposition on Au with high solubility, the voltage profile exhibits zero overpotential with a flat platform, which allows the formation of a surface Li-Au layer eliminating the nucleation barriers for the subsequent Li deposition. The discovery and understanding of the selectivity of Li nucleation opens up the possibility for controlled Li deposition. Thereafter, a nanocapsule was designed consisting of hollow carbon spheres with Au seeds insides. During lithiation, the Au NPs gradually expands and dissolves into the Li phase as can be seen from the *in situ* TEM study. Meanwhile, no Li deposits outside the carbon shell where the nucleation needs additional energy. Such stable encapsulation of Li effectively blocks the dendrite growth, enabling the enhanced cycling stability. It is revealed that the *in situ* EM techniques assist the interfacial investigation of Li growth on various well-built materials, helping the research on Li metal anode to take a step forward.

Another critical challenge for Li anode employment is the continuous formation/dissolution of the SEI. The ideal interfacial layer needs to be chemically stable and mechanically strong, which has been pursued over the years. Fundamental understanding of SEI is the basis. At the Au-Li interface, a SEI film forms from the electrolyte reduction as the *in situ* TEM shown in Fig. 4D[45]. Gas is produced and expands with the active reaction, peeling the SEI from the Au electrode. And, the SEI nucleation and growth can be presented along with the potential sweep[46]. Dendrite-like SEI nucleates and grows rapidly, inducing the irregular SEI surface coverage and nonuniform accessibility of Li^+ to the electrode. Lately, the solid-state electrolyte gains more attention, which replaces the flammable organic electrolyte enabling the safety use of Li anode. The pristine, *ex situ* and *in situ* charged interfaces between Li and the solid electrolyte of amorphous Li phosphorus oxynitride (LiPON) were characterized by TEM (Fig. 4E)[47]. Through the identification from EELS, a disordered interfacial layer evolves to a rocksalt structure along with the formation of Li_2O/Li_2O_2 as the intermediate compound. Besides, an ultrathin interphase can be observed at the cubic $Li_{7-3x}Al_xLa_3Zr_2O_{12}$ (c-LLZO)-Li interface as well[48], suggesting the local reconfiguration of the atomic and electronic structures upon lithiation. The detection of these thin films cannot be readily performed by conventional macroscopic methods, revealing the unique advantage of TEM over SEI investigation. However, as mentioned above, the electron beam disturbs the morphology and components of SEI, which casts a shadow over the visualization of

the intrinsic SEI.

Recently, the cryo-EM technique lifts the veil on the high-resolution imaging of Li and its SEI in their native state at cryogenic conditions[49]. The Li metal was firstly deposited onto a copper TEM grid, then washed with electrolyte and immediately frozen in liquid nitrogen, which retained the electrochemical state with the relevant structural and chemical information preserved. As can be seen in Fig. 4F, the Li dendrite grows as single-crystalline nanowires along different directions. The kink between the growth directions might be due to a variation of the SEI during Li growth, exhibiting defect-free property according to the atomic-resolution imaging. Moreover, the structure and composition of the SEI films was detected and compared in the carbonate-based electrolytes. With the addition of fluoroethylene carbonate (FEC) additive, the SEI layer changes from the mosaic structure to a multilayer structure. The mosaic SEI has a heterogeneous spatial distribution of the inorganic-crystalline and organic-amorphous domains along a single Li dendrite, leading to the nonuniform Li stripping as reported in the following-up work[50]. Conversely, the multilayer SEI with ordered nature ensures the uniform morphology and reduces Li loss during stripping. The utility of cryo-EM is demonstrated on Li observations. Meaningful experiments can potentially be extended to other beam-sensitive materials including S cathode in Li-S batteries.

4 X-Ray Microscopy

To characterize and understand the Li-S interfacial processes across many lengthy scales, a comprehensive multi-modal approach is demanded with the combination of various techniques. TEM provides high-resolution images mainly focusing on a few particles. Besides, because of the unavoidable electron beam, the investigations about many important issues are relatively restricted, such as the PS dissolution and S/Li_2S transformation in electrolytes. In this regard, XRM, which allows an overall and non-destructive imaging under a more realistic experimental environment, is highly complementary.

Early on, researchers employed *in operando* transmission X-ray microscopy (TXM) to probe the sulfide dissolution and re-deposition. Upon discharge, slight size-decrease of a micro-sized S/Super P can be observed, indicating that the soluble PS remains trapped within the cathode matrix[51]. However, without melting S into Super P, the additional TXM results presented complete S dissolution, demonstrating that PS trapping was strongly dependent on the cathode preparation[52]. Moreover, Lin et al. analyzed the PS behaviors in a quantitative manner, who proposed that the dissolution rate of PS exhibited dependence on Li stoichiometry[53]. As shown in Fig. 5A, the S shrinking process can be divided into three regions revealing different PS dissolution rates, including faster rates during the initial and final stages (Regions I and III, respectively) and a slower rate in between (Region II). In terms of Li content, it is revealed that LiS_8 and Li_2S_4 have significantly higher dissolution rates than those between Li_2S_8 and Li_2S_6. Upon charge, size-growth of existing particles takes place prior to new particle formation, which suggests a nucleation-limited PS re-deposition leading to considerable aggregation and dimensional variations during the subsequent cycles. This is different from the *in situ* X-ray fluorescence microscopy (XRF) results collected on the entire *in situ* cell (Fig. 5B)[54]. New spots appear at random locations after charge, corresponding to the newly formed S. Thus, the PS dissolution, nucleation and re-deposition may vary from cases, and be affected by the experimental conditions, such as the cathode material, current density and cut-off voltages. Actually, the current density and temperature indeed play a critical role in determining the PS behaviors, and therefore, the size of S/Li_2S as reported by a latest research[55]. Both the lower temperatures and higher current rates induce the larger overpotentials and lower transport rates. As the *in operando* XRM images depicted in Fig. 5C, a higher number of S nuclei forms at the higher current densities, which grows more uniformly upon discharge. These results expand the understanding of the Li-S reaction mechanism and demonstrate the intermediate PS formation during S/Li_2S transformation.

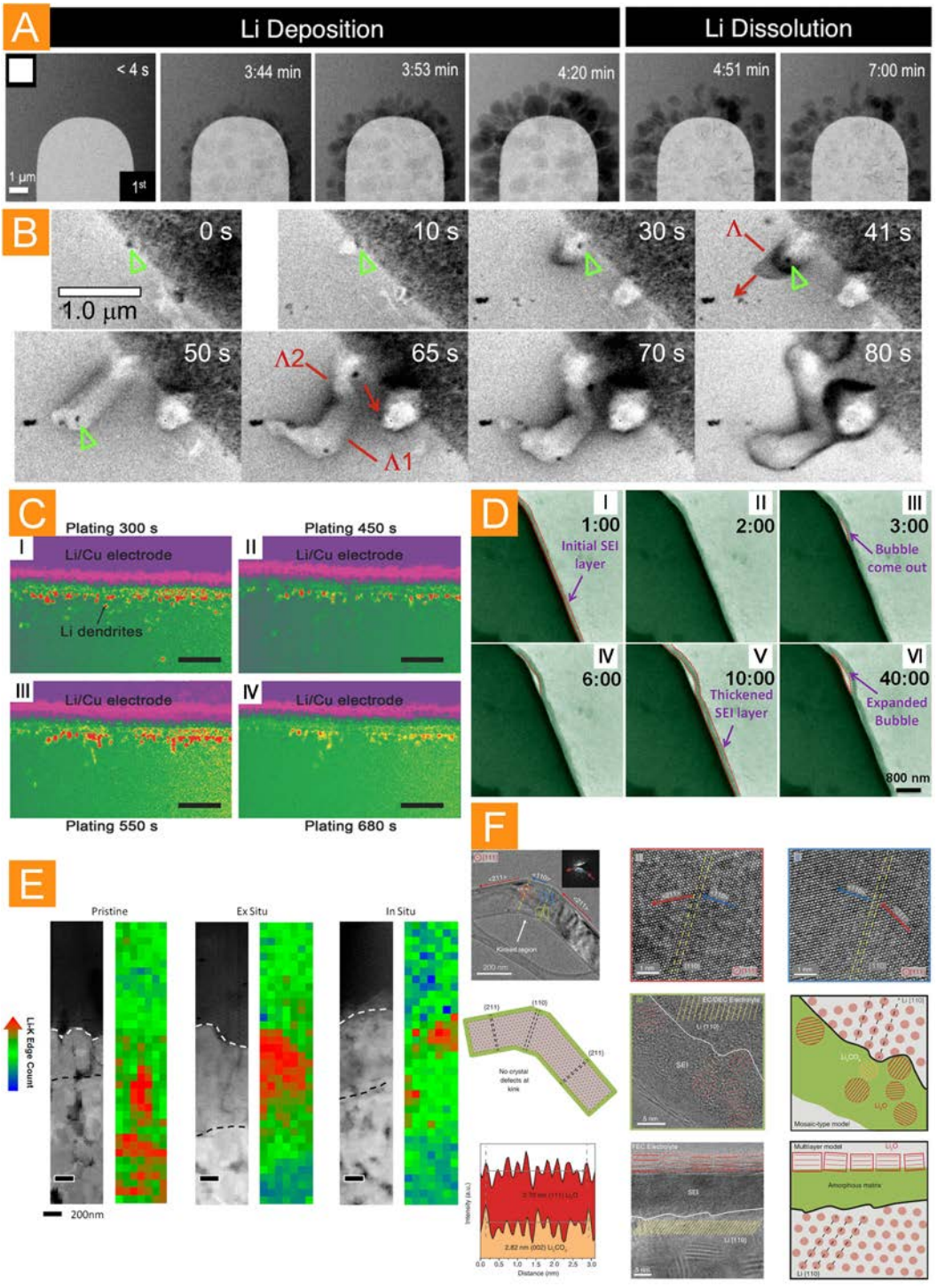

Fig. 4 (A) HAADF images of Li deposition and dissolution at the interface between the Pt working electrode and the $LiPF_6$/PC electrolyte during the first charge/discharge cycle of the *operando* cell[31]. (B) TEM images of the Li whisker growth[33]. (C) A time lapse series of SEM images for the lithium plating process under 0.15 mA·cm^{-2} on the Li/Cu electrode using the LiTFSI/DOL/DME electrolyte with the addition of both Li_2S_8 (0.2 mol·L^{-1}) and $LiNO_3$ (1wt%)[39]. The artificial colors of purple-green-yellow-red represent the different contrasts from bright to dark in grayscale. The dark contrasts of lithium dendrites are colored in red and yellow. Scale bar: 10 μm. (D) Time series of TEM images showing the growth of the SEI film with a gas bubble emerged between the gold electrode and the SEI film[45]. (E) HAADF images of the nanobattery stack along with Li K-edge concentration mapping of pristine, *ex situ*, and *in situ* samples with scale bar represents 200 nm[47]. (F) Atomic-resolution TEM of kinked Li metal dendrite and SEI interface[49].

In addition, the formation of S crystals is observed by *in operando* X-ray radiography (XRR). To eliminate the interference from the pristine solid S/Li_2S, Ballauff et al. mounted the cathode in the cell which was subsequently filled with a PS solution[56]. After the first charging, macroscopic crystals of S deposit like dendrite (Fig. 5D), which can be assigned to rhombic α- and monoclinic β-S from their characteristic crystal habit. The charge transfer process of S occurs rapidly, while of Li_2S exhibits a broad distribution of relaxation time. This proves that it is the inhibited dissolution and slow precipitation of Li_2S limits the reaction kinetics, representing a major issue in Li-S batteries. They further substantiated the formation of S dendrites on a reduced graphene oxide (rGO)/carbon monolith cathode[57]. Moreover, other macroscopic phenomena were observed by *in operando* XRR. An electrolyte ring appears between the separator and Li anode hole, shrinks and expands periodically during serial charge and discharge processes, driven by the concentration gradient and property changes of the electrolyte. And, at the end of each discharge step, a reaction front forms and quickly propagates from Li anode to carbon cathode, due to the rapid movement of high amount of Li^+. More information in Li-S mechanism study is provided through multidimensional analyses for Li-S batteries.

To spatially examine the behaviors on S cathode, 3D X-ray tomography (XRT) was introduced to real-time track the morphology evolution across multiple cycles. It is shown that the S mass transport rate limits the electrochemical reaction, causing uneven distribution and aggregation of S within thick film cathodes[58]. In a thinner film with a smaller particle size and a lower mass loading, almost all of the S particles disappear after discharge as visualized by the *in situ* XRT[59]. However, only a small fraction of S re-deposits upon charge, indicating that Li_2S formation may be the capacity-limiting step. That is similar to the conclusion made by Balluaff et al. uncovering the reaction kinetics and fading mechanism of Li-S electrochemistry[56].

On Li anode, XRT shows the cross-sections of symmetric Li cells cycled to various stages (Fig. 5E). Subsurface structures identified as crystalline impurities were detected at the electrolyte/electrode interfaces, which grew into dendrites protruding out after cycles[60]. Suppressing the nucleation of these subsurface structures is the key to Li interface optimization. Recently, *in operando* synchrotron XRT was employed to record the interfacial evolution of InLi-anode and sulfide-solid-electrolyte[61]. Obvious InLi protrusion and cavity/void are developed during discharge and charge at the interfaces, which can be regarded as the direct evidence of the interfacial deterioration undoubtedly damaging the overall electrochemical performance. Using *in situ*/*in operando* XRM, the aforementioned works provide fundamental understanding of the reaction mechanism on both S cathodes and Li anodes. They focus more on the morphology and component evolution of the overall electrode, including solid-product formation/dissolution at macroscopic scale and the complex soluble PS behaviors in electrolytes, which adds to our knowledge on the battery level for further development.

5 Optical Microscopy

Using *in operando* OM, Cui et al. visualized the formation and distribution of PS in Li-S batteries by simply comparing the electrolyte colors[62]. In Fig. 6A, during the discharge process, the electrolyte turns from colorless to grey, brown yellow, and back to light yellow, revealing that the content of PS initially increases and then decreases. During the subsequent charge, the color becomes increasingly dark, indicating the increasing amount of PS in the electrolyte. The modified Li-S batteries, employing the S-polymer poly(3,4-ethylene-dioxythiophene) (PEDOT) composite cathode and a Nafion coated separator, were further assembled, where a low grey level can be detected during the whole discharge/charge processes. These observations present direct evidence of the PS dissolving and trapping, exhibiting a clever use of *in operando* OM in Li-S batteries.

Besides, *in operando* OM is a suitable tool to visualize macroscopic phenomena like dendrite growth on Li anode. The morphology evolution of the inter-

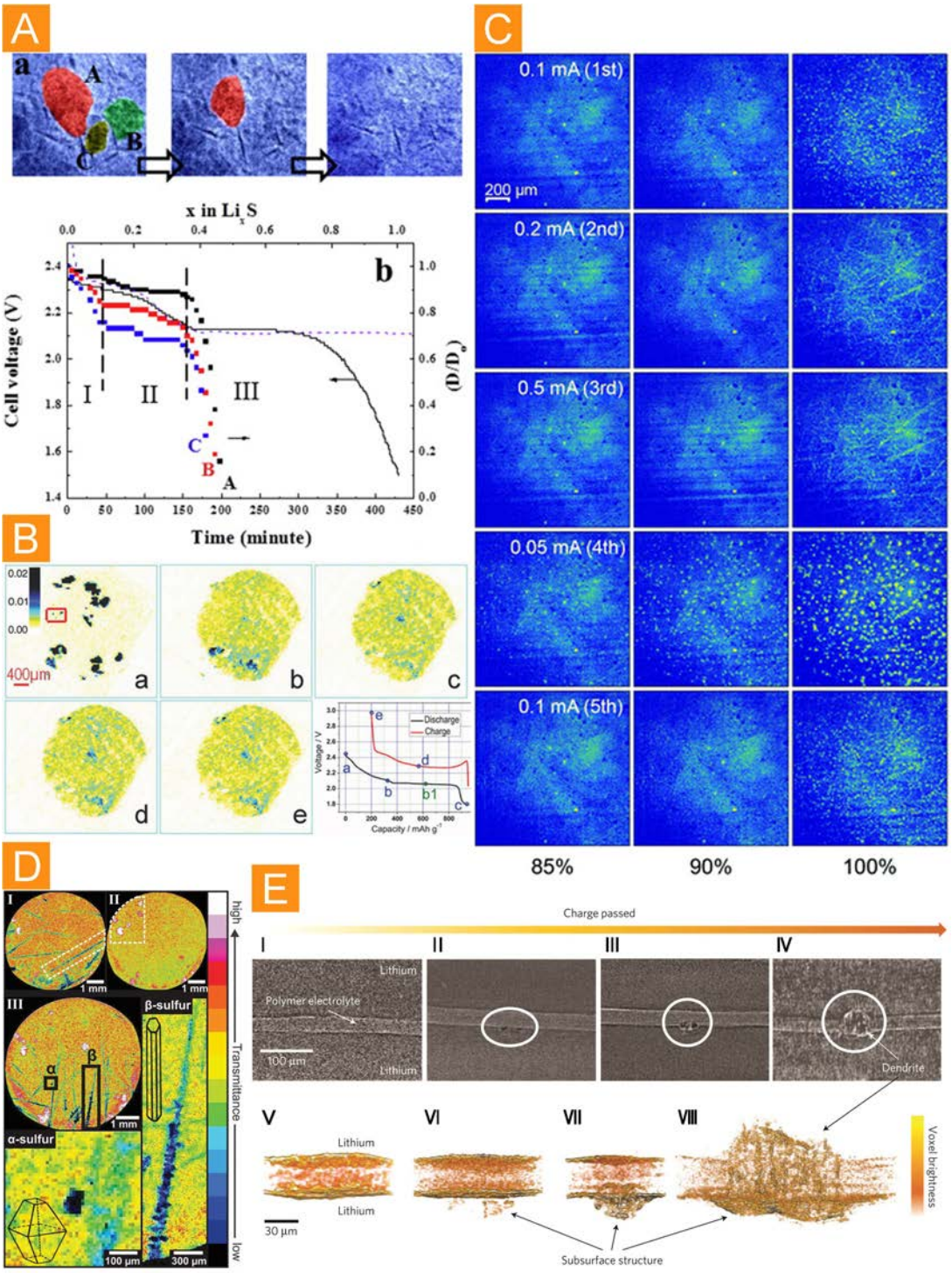

Fig. 5 (A) TXM analysis of a S electrode subjected to a deep electrochemical lithiation[53]. (B) *In situ* 2D-XRF images collected on the entire *in situ* cell window region. Each image was obtained during *in situ* cell discharged/charged as labeled on the charge-discharge curve. The color at each pixel in the image reflects the concentration of the sulfur element, the darker the color, the higher the concentration of sulfur element[54]. (C) Sequential *operando* X-ray microscopic images of the cathode at different charging rates[55]. (D) X-ray images of fully charged (I) and discharged (II) states of the Li-S cell of the 2nd cycle and fully charged state of the 1st cycle (III). The respective crystal habit of α- and β-S is also inserted into the magnified images (α: rhombic; β: monoclinic). The color legend on the right is used for all X-ray images in this work[56]. (E) XRT slices showing the cross-sections of symmetric lithium cells cycled to various stages[60].

faces between Li and various kinds of electrolytes can be directly observed under OM. In 1997, the depositions of Li were compared in the liquid (PC+$LiClO_4$), solid polymer [poly(ethylene oxide) (PEO) +$LiClO_4$], and gel (PEO+PC+$LiClO_4$) electrolytes[63]. Smooth and uniform deposition can only be acquired in the gel electrolyte possessing the advantages of both high conductivity and solid-molecule immobility. Later on, the ionic liquid of lithium bis(triuoromethanesulfonyl) amide in 1-ethyl 3-methyl imidazolium bis(triuoromethanesulfonyl)amide (EMImTFSA-LiTFSA) was designed and tested as the electrolyte[64]. The *in operando* OM results showed obvious improvement in the ionic liquid electrolyte in contrast with the liquid one, indicating a compact interfacial layer with no dendrite. Besides, the solvent and salt in the electrolyte affect the interfacial behaviors upon Li deposition[65]. It is shown that the solvents containing a majority of PC more quickly form dendrites. And, the initiation of dendrites is delayed by changing the salt of LiTFSI into $LiPF_6$, which may be due to the trace HF in the latter etching the dendrite growth.

Similarly, Homma et al. found that the initiation period of the dendrite would be shortened with decreasing $LiClO_4$ concentration as well as increasing current density[66]. More interestingly, during the later stage of Li deposition, the whisker dendrite was monitored to swing into random directions. It comes to be known as the kink introduced by the nonuniform stress distribution between Li and the SEI layer. Then, researchers begin to pay more attention on the detailed dynamic processes of Li growth. Using *in situ* OM, Mönig et al. reported that the deposition can occur at the tips or the roots of the growing Li[67]. Almost simultaneously, they observed the segments between the kinks can elongate as well during deposition (Fig. 6B)[68]. At that time, this phenomenon was attributed to the crystalline defects on dendrites, which now is proved to be inexistent by cryo-EM. Therefore, we tend to explain it as the results from incomplete SEI formation and stress release.

Lately, Bazant et al. visualized Li growth in a glass capillary cell and demonstrated a change of mechanism from root-growing mossy Li to tip-growing dendritic Li at the onset of electrolyte diffusion limitation[69]. As shown in Fig. 6C, moss-like Li starts to be deposited in the early stages of electrodeposition. Mossy Li mainly grows from its roots as has been observed earlier. Afterwards, as indicated by the voltage spike, sparse Li dendrites grow explosively from the tips, representing the growth-mode switch from reaction-limited mossy Li to diffusion-limited dendrite Li. This is correlated with the lack of Li salt to form SEI different from that of the mossy Li. Increasing the salt concentration in the electrolyte will avoid dendrite growth by maximizing the Sand's capacity. Thereafter, with the increase of current density, the authors developed three distinct modes to describe Li growth: the root-growing whiskers, the surface-growing mosses and the tip-growing dendrites[70]. This division of whiskers and mosses is similar to their *in situ* TEM report as mentioned in the EM-anode section. At an intermediate current density, the rate of Li deposition is comparable with the rate of SEI formation, leading to the mossy structure without complete SEI coverage. Up to now, three main morphologies of Li have been visualized and discussed under different operating conditions, including kinds of electrolytes containing different solvents, salts, and deposition time, as well as the current density, showing the critical mechanism understanding for the interfacial engineering.

Furthermore, examples of the *in situ* OM visualization are provided contributing to the advances in the Li interface modification. The additives in electrolytes play a key role to the SEI formation and Li^+ solvation. The synergetic effects of PS/$LiNO_3$[71] and FEC/$LiNO_3$[72] were reported to prevent Li dendrite growth and proved by *in situ* OM. Moreover, the implantable SEI can be constructed via precycling Li metal in a LiTFSI-$LiNO_3$-Li_2S_5 ternary salt electrolyte. The symmetrical cell was assembled with the pretreated advanced and commercial Li metal anodes for *in situ* OM observation. As a result, more dendrites form on the surface of the commercial Li electrode. This pretreated advanced Li anode can be fur-

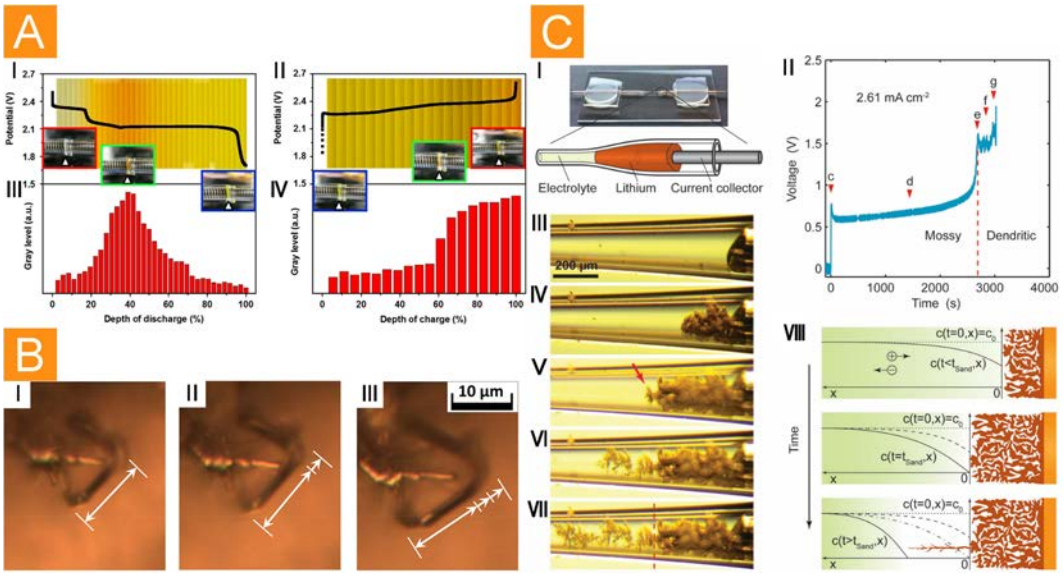

Fig. 6 (A) The discharge and charge curves of the as-made *in operando* lithium-sulfur cell in the potential range of 1.7 ~ 2.6 V and the corresponding change of gray level in the electrolyte with DOD and DOC[62]. (B) *In situ* light microscopic images of needle-like dendrite showing that the segment between the kinks grew in length (marked by white arrows)[68]. (C) *In situ* observations of lithium electrodeposition in a glass capillary revealing the growth mechanisms of lithium electrodeposition[69].

ther transplanted into ether and ester electrolytes to cycle S and $LiNi_{0.5}Co_{0.2}Mn_{0.3}O_2$ (NCM) cathodes, both exhibiting improved cycling performance. Note that this strategy is not limited to LiTFSI-$LiNO_3$-Li_2S_5 ternary salts, delivering new insights into the rational design of Li metal batteries with alternative cathodes and electrolyte systems[73]. The anode coating is another effective way to suppress Li dendrite. Using confocal OM, Tu et al. observed the interfaces on pure Li, amorphous carbon/Li (a-C/Li) and nitrogen-doped a-C/Li (a-CN_x/Li)[74]. And the dendrite growth can be significantly inhibited in the case with a-CN_x/Li. It is found that the doping of N will increase the wetting angle with the electrolyte in favor of the homogeneous Li deposition. Besides, surface-patterned Li (spLi) were prepared with periodically arranged holes on Li electrode[75]. According to the *in situ* OM investigation, it is found that the geometry of the hole has a strong influence on the Li plating/stripping behaviors. Due to the favorable kinetics, Li prefers to deposit into the micro-sized holes with no dendrite and preserves surface morphology. Efforts are continuously needed for the interfacial protection with the rational design, direct evidence and systematic study.

6 Conclusions

In summary, we collate recent research works on the *in situ*/*operando* visualization of the electrode processes in Li-S batteries by means of imaging techniques of AFM, EM, XRM and OM. Fundamental understanding of the important interfacial behaviors is presented, including the morphology evolution, structure changes, reaction kinetics on S cathodes as well as dendrite growth and SEI formation on Li anodes. The electrolyte-dependent and current-dependent electrochemistry is also explored on both electrodes. Widespread utilization of *in situ*/*operando* visualization techniques is still highly required in the field of Li-S batteries. 1) Combined with the spectroscopic characterizations, in-depth works are needed for the recognition of the intermediate PS and the corresponding dynamic transformation. Trying to regulate the reaction kinetics of the sulfides might be an effective approach to trap soluble PS intrinsically. 2) The formation of cathode-electrolyte interphase (CEI) is important for the S cathode protection, however, often overlooked by the researchers. The newly developed cryo-EM exhibits potential applications on the beam-sensitive S cathodes. The detailed visual-

ization of the CEI is helpful to understand the reaction mechanism and therefore promotes the interface optimization. 3) Along with the advances in all-solid-state Li-S batteries, *in situ*/*operando* visualization should be done at interfaces between the nanoarchitected cathode and various solid electrolytes. Atomic-resolution imaging can track the component arrangement and identify the interface layers on both electrodes in solid systems. 4) Though the process in understanding Li dendrite growth has been gained, real-time investigation is still insufficient to prove the growth mechanism. Direct insights into the dynamic evolution of SEI formation and Li deposition should be provided at microscale and nanoscale, further taking into account some external conditions such as the electrolyte, temperature, applied voltage, and current density. Challenges will always exist accompanied by the development of Li-S batteries. The *in situ*/*operando* visualization techniques are the window to the Li-S world, just like the eyes to the soul.

Acknowledgements

The authors acknowledge funding support from the National Key R&D Program of China (Grant No. 2016YFA0202500 and 2016YFB0100100), National Natural Science Fund for Excellent Young Scholars (Grant No. 21722508) and "Hundred Talents Program" from Chinese Academy of Sciences.

References:

[1] Bruce P G, Freunberger S A, Hardwick L J, et al. Li-O_2 and Li-S batteries with high energy storage[J]. Nature Materials, 2012, 11(1): 19-29.

[2] Yin Y X, Xin S, Guo Y G, et al. Lithium-sulfur batteries: Electrochemistry, materials, and prospects[J]. Angewandte Chemie-International Edition, 2013, 52(50): 13186-13200.

[3] Yu S H, Feng X R, Zhang N, et al. Understanding conversion-type electrodes for lithium rechargeable batteries[J]. Accounts of Chemical Research, 2018, 51(2): 273-281.

[4] Agostini M, Lee D J, Scrosati B, et al. Characteristics of Li_2S_8-tetraglyme catholyte in a semi-liquid lithium-sulfur battery[J]. Journal of Power Sources, 2014, 265: 14-19.

[5] Ji X L, Nazar L F. Advances in Li-S batteries[J]. Journal of Materials Chemistry, 2010, 20(44): 9821-9826.

[6] Chen Y, Niu S, Lv W, et al. Promoted conversion of polysulfides by MoO_2 inlaid ordered mesoporous carbons towards high performance lithium-sulfur batteries[J]. Chinese Chemical Letters, 2019, 30(2): 521-524.

[7] Cao R G, Xu W, Lv D P, et al. Anodes for rechargeable lithium-sulfur batteries[J]. Advanced Energy Materials, 2015, 5(16): 142273.

[8] Cheng X B, Zhang R, Zhao C Z, et al. A review of solid electrolyte interphases on lithium metal anode[J]. Advanced Science, 2016, 3(3): 1500213.

[9] Li W J(李文俊), Zheng J Y(郑杰允), Gu L(谷林), et al. Researches on *in-situ* and *ex-situ* characterization techniques in lithium batteries[J]. Journal of Electrochemistry (电化学), 2015, 21(2): 99-114.

[10] Xu R, Lu J, Amine K, et al. Progress in mechanistic understanding and characterization techniques of Li-S batteries[J]. Advanced Energy Materials, 2015, 5(16): 1500408.

[11] Zhao E Y, Nie K H, Yu X Q, et al. Advanced characterization techniques in promoting mechanism understanding for lithium-sulfur batteries[J]. Advanced Functional Materials, 2018, 28(38): 1707543.

[12] Tan J, Liu D N, Xu X, et al. *In situ*/*operando* characterization techniques for rechargeable lithium-sulfur batteries: a review[J]. Nanoscale, 2017, 9(48): 19001-19016.

[13] Zhang G, Zhang Z W, Peng H J, et al. A toolbox for lithium-sulfur battery research: Methods and protocols[J]. Small Methods, 2017, 1: 1700134

[14] Lang S Y, Shi Y, Guo Y G, et al. Insight into the interfacial process and mechanism in lithium-sulfur batteries: An *in situ* AFM study[J]. Angewandte Chemie-International Edition, 2016, 55(51): 15835-15839.

[15] Lang S Y, Shi Y, Guo Y G, et al. High-temperature formation of a functional film at the cathode/electrolyte interface in lithium-sulfur batteries: An *in situ* AFM study [J]. Angewandte Chemie-International Edition, 2017, 56 (46): 14433-14437.

[16] Lang S Y, Xiao R J, Gu L, et al. Interfacial mechanism in lithium-sulfur batteries: How salts mediate the structure evolution and dynamics[J]. Journal of the American Chemical Society, 2018, 140(26): 8147-8155.

[17] Xiong S Z, Xie K, Diao Y, et al. Properties of surface film on lithium anode with $LiNO_3$ as lithium salt in electrolyte solution for lithium-sulfur batteries[J]. Electrochimica Acta, 2012, 83: 78-86.

[18] Xu R, Belharouak I, Zhang X F, et al. Insight into sulfur reactions in Li-S Batteries[J]. ACS Applied Materials Interfaces, 2014, 6(24): 21938-21945.

[19] Zhou W D, Wang C M, Zhang Q L, et al. Tailoring pore size of nitrogen-doped hollow carbon nanospheres for

confining sulfur in lithium-sulfur batteries[J]. Advanced Energy Material, 2015, 5(16): 1401752.

[20] Xu Z L, Huang J Q, Chong W G, et al. *In situ* TEM study of volume expansion in porous carbon nanofiber/sulfur cathodes with exceptional high-rate performance[J]. Advanced Energy Materials, 2017, 7(9): 1602078.

[21] Kim H, Lee J T, Magasinski A, et al. *In situ* TEM observation of electrochemical lithiation of sulfur confined within inner cylindrical pores of carbon nanotubes [J]. Advanced Energy Material, 2015, 5(24): 1501306.

[22] Yu W J, Liu C, Zhang L L, et al. Synthesis and electrochemical lithium storage behavior of carbon nanotubes filled with iron sulfide nanoparticles[J]. Advanced Science, 2016, 3(10): 1600113.

[23] Yuan Y F, Tan G Q, Wen J G, et al. Encapsulating various sulfur allotropes within graphene nanocages for long-lasting lithium storage[J]. Advanced Functional Materials, 2018, 28(38): 1706443.

[24] Tang W, Chen Z X, Tian B B, et al. *In situ* observation and electrochemical study of encapsulated sulfur nanoparticles by MoS_2 flakes[J]. Journal of the American Chemical Society, 2017, 139(29): 10133-10141.

[25] Tan G Q, Xu R, Xing Z Y, et al. Burning lithium in CS_2 for high-performing compact Li_2S-graphene nanocapsules for Li-S batteries[J]. Nature Energy, 2017, 2(7): 17090.

[26] Hwa Y, Seo H K, Yuk J M, et al. Freeze-dried sulfur-graphene oxide-carbon nanotube nanocomposite for high sulfur-loading lithium/sulfur cells[J]. Nano Letters, 2017, 17(11): 7086-7094.

[27] Yang Z Z, Zhu Z Y, Ma J, et al. Phase separation of Li_2S/S at nanoscale during electrochemical lithiation of the solid-state lithium-sulfur battery using *in situ* TEM [J]. Advanced Energy Material, 2016, 6(20): 1600806.

[28] Qiu Y C, Rong G L, Yang J, et al. Highly nitridated graphene-Li_2S cathodes with stable modulated cycles[J]. Advanced Energy Materials, 2015, 5(23): 1501369.

[29] Luntz A C, Voss J, Reuter K, et al. Interfacial challenges in solid-state Li ion batteries[J]. Journal of Physical Chemistry Letters, 2015, 6(22): 4599-4604.

[30] Marceau H, Kim C S, Paolella A, et al. *In operando* scanning electron microscopy and ultraviolet-visible spectroscopy studies of lithium/sulfur cells using all solid-state polymer electrolyte[J]. Journal of Power Sources, 2016, 319: 247-254.

[31] Mehdi B L, Qian J, Nasybulin E, et al. Observation and quantification of nanoscale processes in lithium batteries by *operando* electrochemical (S)TEM[J]. Nano Letters, 2015, 15(3): 2168-2173.

[32] Leenheer A J, Jungjohann K L, Zavadil K R, et al. Lithium electrodeposition dynamics in aprotic electrolyte observed *in situ* via transmission electron microscopy[J]. ACS Nano, 2015, 9(4): 4379-4389.

[33] Kushima A, So K P, Su C, et al. Liquid cell transmission electron microscopy observation of lithium metal growth and dissolution: Root growth, dead lithium and lithium flotsams[J]. Nano Energy, 2017, 32: 271-279.

[34] Orsini F, Pasquier A D, Beaudoin B, et al. *In situ* scan ning electron microscopy (SEM) observation of interfaces within plastic lithium batteries[J]. Journal of Power Sources, 1998, 76(1): 19-29.

[35] Aurbach D, Gofer Y, et al. The correlation between surface chemistry, surface morphology, and cycling efficiency of lithium electrodes in a few polar aprotic systems[J]. Journal of Electrochemical Society, 1989, 136(11): 3198-3205.

[36] Aurbach D, Gofer Y, Moshe B Z, et al. The behavior of lithium electrodes in propylene and ethylene carbonate: The major factors that influence Li cycling efficiency[J]. Journal of Electroanalytical Chemistry, 1992, 339 (1/2): 451-471.

[37] Dolle M, Sannier L, Beaudoin B, et al. Live scanning electron microscope observations of dendritic growth in lithium/polymer cells[J]. Electrochemical and Solid-State Letters, 2002, 5(12): A286-A289.

[38] Sagane F, Shimokawa R, Sano H, et al. *In-situ* scanning electron microscopy observations of Li plating and stripping reactions at the lithium phosphorus oxynitride glass electrolyte/Cu interface[J]. Journal of Power Sources, 2013, 225: 245-250.

[39] Rong G L, Zhang X Y, Zhao W, et al. Liquid-phase electrochemical scanning electron microscopy for *in situ* investigation of lithium dendrite growth and dissolution[J]. Advanced Materials, 2017, 29(13): 1606187.

[40] Li Y J, Jiao J Y, Bi J P, et al. Controlled deposition of Li metal[J]. Nano Energy, 2017, 32: 241-246.

[41] Xin S, Guo Y G, Wan L J, et al. Nanocarbon networks for advanced rechargeable lithium batteries[J]. Accounts of Chemical Research, 2012, 45(10): 1759-1769.

[42] Yang C P, Yin Y X, Zhang S F, et al. Accommodating lithium into 3D current collectors with a submicron skeleton towards long-life lithium metal anodes[J]. Nature Communications, 2015, 6: 8058.

[43] Zheng G Y, Lee S W, Liang Z, et al. Interconnected hollow carbon nanospheres for stable lithium metal anodes [J]. Nature Nanotechnology, 2014, 9(8): 618-623.

[44] Yan K, Lu Z D, Lee H W, et al. Selective deposition and

stable encapsulation of lithium through heterogeneous seeded growth[J]. Nature Energy, 2016, 1(3): 16010.

[45] Zeng Z Y, Liang W I, Liao H G, et al. Visualization of electrode-electrolyte interfaces in $LiPF_6$/EC/DEC electrolyte for lithium ion batteries via *in situ* TEM[J]. Nano Letters, 2014, 14(4): 1745-1750.

[46] Sacci R L, Dudney N J, More K L, et al. Direct visualization of initial SEI morphology and growth kinetics during lithium deposition by *in situ* electrochemical transmission electron microscopy[J]. Chemical Communication, 2014, 50(17): 2104-2107.

[47] Wang Z Y, Santhanagopalan D, Zhang W, et al. *In situ* STEM-EELS observation of nanoscale interfacial phenomena in all-solid-state batteries[J]. Nano Letters, 2016, 16(6): 3760-3767.

[48] Ma C, Cheng Y Q, Yin K B, et al. Interfacial stability of Li metal-solid electrolyte elucidated via *in situ* electron microscopy[J]. Nano Letters, 2016, 16(11): 7030-7036.

[49] Li Y Z, Li Y B, Pei A, et al. Atomic structure of sensitive battery materials and interfaces revealed by cryo-electron microscopy[J]. Science, 2017, 358(6362): 506-510.

[50] Li Y Z, Huang W, Li Y B, et al. Correlating structure and function of battery interphases at atomic resolution using cryoelectron microscopy[J]. Joule, 2018, 2(10): 2167-2177.

[51] Nelson J, Misra S, Yang Y, et al. *In operando* X-ray diffraction and transmission X-ray microscopy of lithium sulfur batteries[J]. Journal of the American Chemical Society, 2012, 134(14): 6337-6343.

[52] Nelson J, Yang Y, Misra S, et al. Identifying and managing radiation damage during *in situ* transmission X-ray microscopy of Li-ion batteries[M]. X-Ray Nanoimaging: Instruments and Methods, Proceedings of SPIE, 2013, 8851: UNSP 88510B.

[53] Lin C N, Chen W C, Song Y F, et al. Understanding dynamics of polysulfide dissolution and re-deposition in working lithium-sulfur battery by *in-operando* transmission X-ray microscopy[J]. Journal of Power Sources, 2014, 263: 98-103.

[54] Yu X Q, Pan H L, Zhou Y N, et al. Direct observation of the redistribution of sulfur and polysufides in Li-S batteries during the first cycle by *in situ* X-ray fluorescence microscopy[J]. Advanced Energy Materials, 2015, 5(16): 1500072.

[55] Yu S H, Huang X, Schwarz K, et al. Direct visualization of sulfur cathodes: New insights into Li-S batteries via *operando* X-ray based methods[J]. Energy Environmental Science, 2018, 11(1): 202-210.

[56] Risse S, Jafta C J, Yang Y, et al. Multidimensional *operando* analysis of macroscopic structure evolution in lithium sulfur cells by X-ray radiography[J]. Physical Chemistry Chemical Physics, 2016, 18(15):10630-10636.

[57] Yang Y, Risse S, Mei S, et al. Binder-free carbon monolith cathode material for *operando* investigation of high performance lithium-sulfur batteries with X-ray radiography[J]. Energy Storage Materials, 2017, 9: 96-104.

[58] Yermukhambetova A, Tan C, Daemi S R, et al. Exploring 3D microstructural evolution in Li-Sulfur battery electrodes using *in-situ* X-ray tomography[J]. Scientific Reports, 2016, 6: 35291.

[59] Tan C, Daemi S R, Brett D J L, et al. Investigating the three-dimensional microstructural characteristics of lithium-sulfur electrodes with X-ray micro-tomography[J]. ECS Transactions, 2017, 77(11): 447-455.

[60] Harry K J, Hallinan D T, Parkinson D Y, et al. Detection of subsurface structures underneath dendrites formed on cycled lithium metal electrodes[J]. Nature Materials, 2013, 13(1): 69-73.

[61] Sun F, Dong K, Osenberg M, et al. Visualizing morphological and compositional evolution of interface of In-Li-anode|thio-LISION electrolyte in all-solid-state Li-S cell by *in operando* synchrotron X-ray tomography and energy dispersive diffraction[J]. Journal of Materials Chemistry A, 2018, 6(45): 22489-22496.

[62] Sun Y M, Seha Z W, Li W Y, et al. *In-operando* optical imaging of temporal and spatial distribution of polysulfides in lithium-sulfur batteries[J]. Nano Energy, 2015, 11: 579-586.

[63] Osaka T, Homma T, Momma T, et al. *In situ* observation of lithium deposition processes in solid polymer and gel electrolytes[J]. Journal of Electroanalytical Chemistry, 1997, 421(1/2): 153-156.

[64] Howlett P C, MacFarlane D R, Hollenkamp A F, et al. A sealed optical cell for the study of lithium-electrode|electrolyte interfaces[J]. Journal of Power Sources, 2003, 114: 277-284.

[65] Crowther O, West A C. Effect of electrolyte composition on lithium dendrite growth[J]. Journal of The Electrochemical Society, 2008, 155(11): A806-A811.

[66] Nishikawa K, Mori T, Tetsuo Nishida, et al. *In situ* observation of dendrite growth of electrodeposited Li metal [J]. Journal of The Electrochemical Society, 2010, 157 (11): A1212-A1217.

[67] Steiger J, Kramer D, Mönig R. Microscopic observations of the formation, growth and shrinkage of lithium moss during electrodeposition and dissolution[J]. Electrochimica Acta, 2014, 136: 529-536.

[68] Steiger J, Kramer D, Mönig R. Mechanisms of dendritic growth investigated by *in situ* light microscopy during electrodeposition and dissolution of lithium[J]. Journal of Power Sources, 2014, 261: 112-119.

[69] Bai P, Li J, Brushett F R, et al. Transition of lithium growth mechanisms in liquid electrolytes[J]. Energy Environmental Science, 2016, 9(10): 3221-3229.

[70] Bai P, Guo J Z, Wang M, et al. Interactions between lithium growths and nanoporous ceramic separator[J]. Joule, 2018, 2(11): 1-16.

[71] Li W Y, Yao H B, Yan K, et al. The synergetic effect of lithium polysulfide and lithium nitrate to prevent lithium dendrite growth[J]. Nature Communications, 2015, 6: 7436.

[72] Zhang X Q, Chen X, Cheng X B, et al. Highly stable lithium metal batteries enabled by regulating the solvation of lithium ions in nonaqueous electrolytes[J]. Angewandte Chemie-International Edition, 2018, 57(19): 5301-5305.

[73] Cheng X B, Yan C, Chen X, et al. Implantable solid electrolyte interphase in lithium-metal batteries[J]. Chem, 2017, 2: 258-270.

[74] Zhang Y J, Bai W Q, Wang X L, et al. *In situ* confocal microscopic observation on inhibiting the dendrite formation of a-CN_x/Li electrode[J]. Journal of Materials Chemistry A, 2016, 4(40): 15597-15604.

[75] Li Q, Quan B B, Li W J, et al. Electro-plating and stripping behavior on lithium metal electrode with ordered three-dimensional structure[J]. Nano Energy, 2018, 45: 463-470.

锂硫电池中电极过程的原位可视化研究进展

郎双雁[1,2],胡新成[1,2],文　锐[1,2*],万立骏[1,2*]

(1. 中国科学院分子纳米结构与纳米技术重点实验室,北京分子科学国家研究中心, 分子科学科教融合卓越中心, 中国科学院化学研究所, 北京 100190; 2. 中国科学院大学 北京 100049)

摘要:锂硫电池被认为是极具应用潜力的下一代能源存储器件之一. 在锂硫电池中,对电极-电解质界面物质结构和演变规律的深入探究及认知对其进一步发展至关重要. 本文结合多种原位可视化技术, 包括扫描探针显微术、电子显微术、X 射线以及光学显微术,概述了近年来在锂硫电池中界面成像分析的研究进展. 主要讨论了在硫正极界面、硫/硫化锂演变、多硫化物溶解以及在锂负极界面、固液界面层形成、锂沉积行为等问题,有助于理解锂硫反应的基本原理并提出优化方案.

关键词:原位可视化技术;锂硫电池;电极-电解质界面;锂负极;电极过程